ELSEVIER

Biophysical Chemistry 84 (2000) 177–188

Biophysical Chemistry

www.elsevier.nl/locate/bpc

Interactions of proteins in aqueous electrolyte solutions from fluorescence anisotropy and circular-dichroism measurements

C.O. Anderson[a], J.F.M. Niesen[1,a], H.W. Blanch[a,*], J.M. Prausnitz[a,b]

[a] *Department of Chemical Engineering, University of California, Berkeley, CA 94720, USA*
[b] *Chemical Sciences Division, Lawrence Berkeley National Laboratory, University of California, Berkeley, CA 94720, USA*

Received 1 November 1999; received in revised form 29 December 1999; accepted 29 December 1999

Abstract

Understanding aqueous protein–protein interactions is crucial for the development of a molecular–thermodynamic model for salt-induced protein precipitation. In addition, protein interactions are important in many disease states, including cataract formation and α-amyloid diseases. Fluorescence anisotropy provides a means to measure intermolecular interactions. In this work, monomer–dimer equilibrium of the peptide T4 LYS(11–36) was studied by fluorescence anisotropy over the pH range 4–7 and the NaCl concentration range 0.0–1.0 M, in a 25 mM sodium phosphate buffer. This 26 amino-acid peptide is derived from the β-sheet region of the T4 lysozyme molecule and has the potential to form amyloid fibrils. The association constant for dimerization increases with rising pH and ionic strength. The potential of mean force for peptide–peptide interactions was calculated from these association constants. Circular-dichroism measurements show that the peptide becomes more structured as the pH rises, possibly contributing to increased association.

Keywords: Protein–protein interactions; Specific interactions; Potentials of mean force; Fluorescence polarization anisotropy; Amyloid fibrillogenesis; Circular-dichroism

1. Introduction

A quantitative understanding of aqueous protein–protein interactions has several applications. One important application is to establish a molecular-based theory for salt-induced protein precipitation, a common first-step method for protein recovery. At present, most salting-out procedures are based on experience, trial-and-error methods and empirical correlations. Consequently, selection of a good separation procedure may be labor-intensive and costly. Through measurements of protein–protein interactions under di-

* Corresponding author. Tel.: +1-510-643-7255; fax: +1-510-643-1228.
E-mail address: blanch@socrates.berkely.edu (H.W. Blanch)
[1] Present address: Schering AG, 13342 Berlin, Germany.

0301-4622/00/$ - see front matter
PII: S0301-4622(00)00115-0

lute-solution conditions, a model can be developed for predicting phase separation of proteins in concentrated electrolyte solutions.

Protein–protein interactions are also important in certain disease states. In Alzheimer's disease, for example, it has been hypothesized that monomers or dimers of the Aβ protein associate to form protofibrils with β-sheet structure [1–3]. These protofibrils lengthen to full-length fibrils that form clusters. In time, the plaques which accompany the disease are observed. There are other diseases that involve protein aggregation and deposition, including cataract formation, Huntington's disease and bovine spongiform encephalopathy (Mad Cow disease). Determining the intermolecular forces that lead to protein aggregation can thus play a role in understanding how these diseases arise.

This work is concerned with protein–protein interactions that may be related to β-amyloid formation. Various forms of lysozyme are capable of undergoing amyloid fibrillogenesis. Human lysozyme variants have been shown to form fibrils with β-structure [4]. In addition, peptide fragments from the β-sheet region of hen egg-white lysozyme associate to form an extensive β-structure [5]. In this work, the interactions that lead to β-amyloid fibrillogenesis are examined using fluorescence-anisotropy measurements of the peptide T4 LYS(11–36), a 26 amino-acid peptide derived from the β-sheet region of the T4 lysozyme. Circular-dichroism spectropolarimetry is used to determine whether the secondary structure of the T4 lysozyme peptide plays a role in association. The two-body interactions between peptide molecules are modeled using a potential of mean force composed of a repulsive hard-sphere potential, an electric double-layer-repulsion potential, an attractive dispersion potential and an attractive site-specific square-well potential.

2. Fluorescence anisotropy and Brownian motion

Changes in the association state of molecules are reflected by changes in molecular motion. Fluorescence-anisotropy measurements are useful for investigating these changes provided that fluorescently-labeled molecules are available. The equation governing rotational Brownian motion is [6–8]:

$$D_r = \frac{RT}{6\eta V} \tag{1}$$

where D_r is the molecular rotational diffusion coefficient, R is the universal gas constant, T is the absolute temperature, η is the solution viscosity and V is the molar volume, given by [9,10]:

$$V = M(\bar{v} + h) \tag{2}$$

Here, M is the molecular weight of the molecule, $\bar{v}$ is the partial specific volume and h is the hydration. As the solution temperature increases, the molecules tumble at an increasing rate; as the solution viscosity or the particle volume increase, the molecules rotate more slowly. Association of molecules results in an increase in particle volume.

While Eq. (1) fully describes rotational diffusion, it cannot be used directly for analysis of fluorescence-anisotropy data. Instead, we use the Perrin equation that relates anisotropy to molecular motion [11]:

$$A = \frac{A_o}{1 + (RT\tau/\eta V)} \tag{3}$$

Here, A_o is a constant representing the anisotropy in the absence of molecular motion and τ is the fluorescence lifetime of the fluorophore used. In this work, the effect of peptide concentration on the measured anisotropy is used to determine the association state of the peptides.

3. Measurement of fluorescence anisotropy

Fluorescence anisotropy is measured by first exciting a molecule with vertically polarized light, then observing the fluorescence intensity of emitted light passing through a polarizer held alternately parallel to and perpendicular to the direction of polarization of the incident light [7,10].

The anisotropy is related to these intensities by [11]:

$$A = \frac{I_{\parallel} - I_{\perp}}{I_{\parallel} + 2I_{\perp}} \tag{4}$$

where $I_{\parallel}$ is the intensity of emitted light measured in the direction parallel to excitation and $I_{\perp}$ is the intensity of emitted light measured in the direction perpendicular to excitation.

4. Relation of anisotropy to the association constant, K_a

Anisotropy is measured as a function of peptide concentration to provide information on monomer–dimer equilibrium. The sample solutions contain both fluorescently-labeled and unlabeled peptide molecules. The use of unlabeled peptides serves to keep the total peptide concentration high while lowering the risk of energy transfer between fluorophores. Thus, reversible binding of monomers leads to three types of dimer molecules:

$$L + L \overset{K_{L_2}}{\Leftrightarrow} L_2$$

$$L^* + L \overset{K_{L^*L}}{\Leftrightarrow} L^*L$$

$$L^* + L^* \overset{K_{L_2^*}}{\Leftrightarrow} L_2^* \tag{5}$$

where L is the unlabeled T4 lysozyme peptide (11–36) and L^* is the labeled peptide. (The peptide is labeled with 7-methoxycoumarin-3-carboxylic acid.) A 1:9 molar ratio of labeled to unlabeled peptide was chosen to ensure that the concentration of the dimer L_2^* is small compared to the concentration of the other dimers, and can therefore be neglected. This simplification is necessary to solve the system of equations which would otherwise be underdetermined. At equilibrium, the remaining association constants in Eq. (5) are given by:

$$K_{L_2} = \frac{[L_2]}{[L]^2}$$

$$K_{L^*L} = \frac{[L^*L]}{[L^*]\cdot[L]} \tag{6}$$

We assume that the fluorescent label does not affect the interactions between the peptide molecules. Association would only be altered if the label was located at the site of interaction, or if the label altered the conformation of the peptide. The label was placed on the N-terminus to avoid these possibilities. Thus, the two association constants in Eq. (6) are equal and equivalent to K_a.

For a mixture of monomers and dimers carrying the same fluorophore [12]:

$$A = A_f F_f + A_b F_b$$

$$F_f + F_b = 1 \tag{7}$$

where the subscript f denotes molecules in the monomer (free) form and b denotes molecules in the dimer (bound) form. A_f is the infinite-dilution anisotropy, while A_b is the limiting value at very high peptide concentrations where all molecules are in the bound form. F_b, the fraction of labeled molecules in the dimer form, is given by:

$$F_b = \frac{[L^*L]}{[L^*]_T} \tag{8}$$

where $[L^*]_T$ is the total concentration of labeled peptide in the mixture.

The mass-balance equations for this system are:

$$[L^*]_T = [L^*] + [L^*L] \tag{9}$$

$$[L]_T = [L] + [L^*L] + 2[L_2] \tag{10}$$

$$[L^*]_T = \lambda^*[\Lambda]_T \tag{11}$$

$$[L]_T = \lambda[\Lambda]_T \tag{12}$$

where $[L^*]_T$ is the total unlabeled peptide concentration,

$$[\Lambda]_T = [L^*]_T + [L]_T$$

is the total molar peptide concentration, λ^* is the mole fraction of labeled peptide, and λ is the mole fraction of unlabeled peptide. Combination of Eqs. (6)–(12) relates the experimental anisotropy to the association constant:

$$[\Lambda]_T = \frac{\left[\left(\frac{A-A_f}{A_b-A_f}\right)+\left(\frac{A-A_f}{A_b-A_f}\right)^2\right]}{K_a\cdot\left[1-\left(\frac{A-A_f}{A_b-A_f}\right)\right]^2\cdot\left[\lambda-\left(\frac{A-A_f}{A_b-A_f}\right)\lambda^*\right]} \quad (13)$$

$[L^*]_T$ and $[L]_T$ are measured experimentally to obtain λ^*, λ, and $[\Lambda]_T$. Parameters A_f and A_b are estimated by plotting the experimental anisotropy, A vs. $\log [\Lambda]_T$ and extrapolating (see Fig. 1). Non-linear least-squares regression (using the program SigmaPlot) is used to fit the data to Eq. (13) and to obtain the association constant for dimerization, K_a.

5. Calculation of the potential of mean force

The association constant can be related to the sum of several contributions to the potential of mean force. The association in this system is assumed to be driven primarily by specific attractive interactions between the peptide molecules [13,14]. These attractive interactions arise due to hydrophobic forces, hydrogen-bond formation, and short-range attractive electrostatic forces [15]. The potential of mean force also depends on the size and net charge of the peptide molecules. Thus, the potential of mean force is given by a sum of pairwise potentials:

$$W(r) = W_{\text{hs}}(r) + W_{\text{elec}}(r) + W_{\text{disp}}(r) + W_{\text{spec}}(r) \quad (14)$$

where r is the center-to-center distance between peptide molecules. Here, $W_{\text{hs}}(r)$ is the peptide hard-sphere potential, $W_{\text{elec}}(r)$ is the electric double-layer-repulsion potential, and $W_{\text{spec}}(r)$ is a square-well potential that accounts for specific interactions between two peptide molecules. Derjaguin–Landau–Verwey–Overbeek (DLVO) theory accounts for the first three terms in the sum [16].

The hard-sphere potential is given by [16]:

$$W_{\text{hs}}(r) = \begin{cases} \infty & \text{for} \quad r \le \sigma \\ 0 & \text{for} \quad r > \sigma \end{cases} \quad (15)$$

where σ is the effective spherical diameter of the peptide. The electric double-layer-repulsion potential is derived from Debye–Hückel theory [16]:

$$W_{\text{elec}}(r) = \frac{z^2e^2\exp[-\kappa(r-\sigma)]}{4\pi r\varepsilon_o\varepsilon_r(1+\kappa\sigma/2)^2} \text{ for } r > \sigma \quad (16)$$

where z is the valence of the peptide, e is the unit charge on an electron, $4\pi\varepsilon_o$ is the dielectric permittivity of free space, and ε_r is the relative dielectric permittivity of water; κ is the inverse Debye length given by:

$$\kappa^2 = \frac{2e^2N_{\text{A}}I}{kT\varepsilon_o\varepsilon_r} \quad (17)$$

where N_{A} is Avogadro's number and I is the salt ionic strength. When the ionic strength of the salt is below 0.1 M, it is reasonable to approximate the salt as a point charge. As ionic strength increases, the Debye–Hückel model breaks down

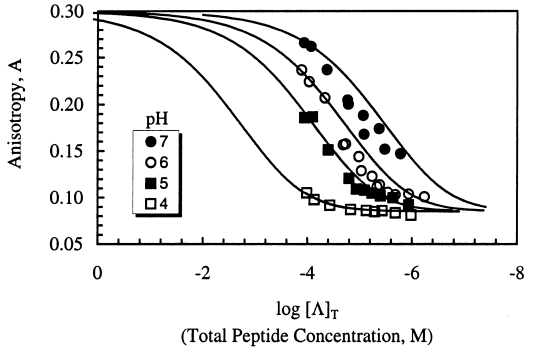

Fig. 1. Anisotropy measurements for T4 LYS(11–36) in a 25 mM sodium phosphate buffer as a function of pH. NaCl concentration is zero. Symbols represent experimental data at 18°C. Solid lines represent extrapolation to infinite dilution (A_f) and to saturation (A_b).

because ionic size becomes significant. Fortunately, however, the effect of ion size in $W_{elec}(r)$ is of minor importance because at high salt concentrations, the electric double-layer repulsion tends to vanish due to screening.

The attractive dispersion potential for these molecules is well approximated by [17]:

$$W_{disp}(r) = -\frac{H}{36}\left(\frac{\sigma}{r}\right)^6 \quad (18)$$

where H is the effective Hamaker constant for the peptide–peptide interaction. The Hamaker constant is primarily a function of the chemical composition of the peptide [17]. The ionic strength has little effect on the dispersion interaction because the time constant for spatial adjustment of ions in the double layer is much larger than that for electronic fluctuations between atoms [18]. The Hamaker constant of a protein is on the order of 5 kT [17].

The site-specific square-well potential developed by Wertheim [19] represents binding between two attractive sites; each site is located on the surface of a distinct peptide molecule. The orientation-dependent potential is given by:

$$\phi(r) = \begin{cases} -\varepsilon_{spec} & \text{for} \quad x < x_c \\ 0 & \text{for} \quad x > x_c \end{cases} \quad (19)$$

where x is the distance between the sites and x_c is the cutoff distance of the attractive potential. The function $\phi(r)$ is orientation-averaged to obtain the spherically symmetric potential $W_{spec}(r)$. To ensure that only dimers are formed, the cutoff distance for sites located on the surfaces of the molecules must be less than or equal to 0.134σ [19]. Since we assume only a monomer–dimer association, this cutoff distance is used in the present work. The square-well depth, ε_{spec}, is a fitting parameter.

The association constant, K_a, is related to the potential of mean force by [20]:

$$K_a = \frac{1}{2}\int_0^\infty S(r)\cdot\exp[-W(r)/kT]\cdot 4\pi r^2 dr \quad (20)$$

where $S(r)$ is defined as:

$$S(r) = \begin{cases} 1 & \text{for} \quad r < r_c \\ 0 & \text{for} \quad r \geq r_c \end{cases} \quad (21)$$

and $r_c = x_c + \sigma$. Values of ζ are calculated from experimental K_a.

6. Results

6.1. Anisotropy measurements

(Experimental details are given in Appendix A) The anisotropy of T4 LYS(11–36) was measured in a 25 mM sodium phosphate buffer at pH 4, 5, 6 and 7; results are shown in Fig. 2. The total peptide concentration, $[\Lambda]_T$, was varied in the range 0.5–160 μM. All measurements were performed at 18°C. Anisotropy increases with rising peptide concentration, signifying greater binding of peptides. At pH 4, anisotropy increases slightly as concentration rises, indicating that little binding occurs at this low pH. As pH rises, the anisotropy becomes a stronger function of concentration, indicating increased binding, as expected, because the isoelectric point of the peptide is pH 9.9.

Figs. 3 and 4 show the ionic-strength dependence of the anisotropy at pH 4 and 5. At pH 4, increasing the ionic strength slightly to 0.1 M has little effect on the concentration dependence of

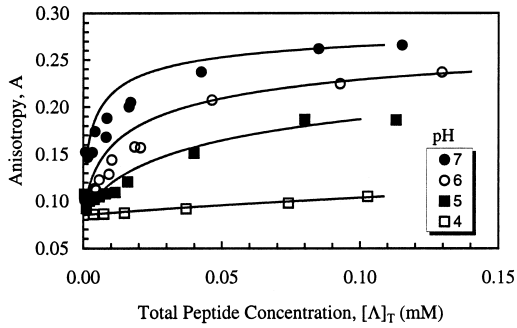

Fig. 2. Anisotropy measurements for T4 LYS(11–36) in a 25 mM sodium phosphate buffer as a function of pH. NaCl concentration is zero. Symbols represent experimental data at 18°C. Solid lines represent the best-fit curves using Eq. (13).

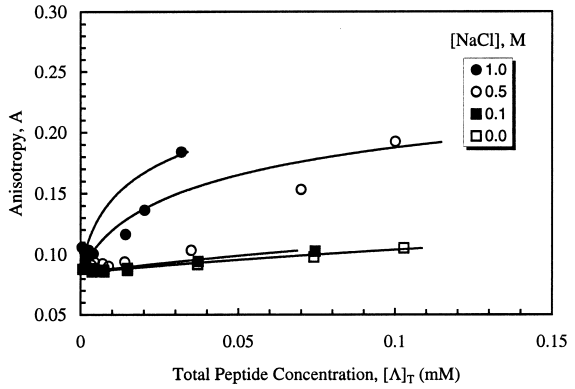

Fig. 3. Anisotropy measurements for T4 LYS(11–36) in a 25 mM sodium phosphate buffer at pH 4 as a function of NaCl concentration. Symbols represent experimental data at 18°C. Solid lines represent the best-fit curves using Eq. (13).

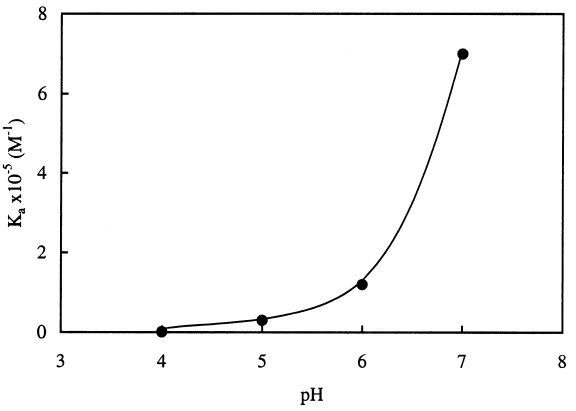

Fig. 5. Association constant, K_a, for dimerization of T4 LYS(11–36) at 18°C as a function of pH. NaCl concentration is zero. A spline fit is used to guide the eye.

anisotropy. As ionic strength increases further, a significant concentration dependence is observed. Similar behavior is observed at pH 5.

6.2. Association constants

Association constants for dimerization of T4 LYS(11–36) are calculated by fitting the experimental data with Eq. (13). For these measurements, $\lambda = 0.9$ and $\lambda^* = 0.1$. Parameters A_f and A_b are estimated by plotting the experimental anisotropy, A vs. $\log [\Lambda]_T$ and extrapolating (see Fig. 1). A_f and A_b are 0.085 and 0.3, respectively; they are assumed independent of pH and salt concentration. The best-fit curves are shown in Figs. 2–4. Fig. 5 shows the association constant for peptide dimerization as a function of pH. The association constant increases with pH. The association constants shown in Fig. 6 are for measurements at pH 4 and 5 with sodium-chloride concentrations in the range 0.0–1.0 M. The association constant increases with salt concentration.

6.3. Potential of mean force

The potential of mean force is calculated using

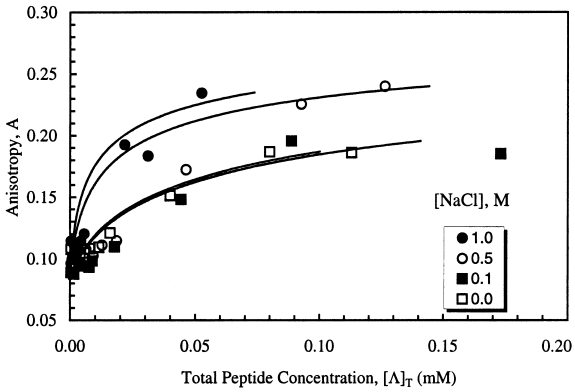

Fig. 4. Anisotropy measurements for T4 LYS(11–36) in a 25 mM sodium phosphate buffer at pH 5 as a function of NaCl concentration. Symbols represent experimental data at 18°C. Solid lines represent the best-fit curves using Eq. (13).

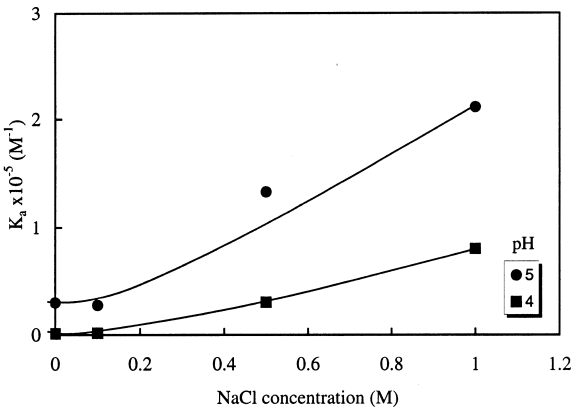

Fig. 6. Association constant, K_a, for dimerization of T4 LYS(11–36) at 18°C as a function of NaCl concentration. A spline fit is used to guide the eye.

Table 1
Net electric charge of T4 LYS(11–36) as a function of pH (calculated from free-amino-acid titration in 0.1 M KCl)

pH	4	5	6	7
Net charge	+3.1	+2.5	+2.1	+1.7

Eqs. (14)–(21). The peptide diameter is 18.8 Å (see Appendix A). The peptide charge, shown in Table 1, was calculated using results from free-amino-acid titration in 0.1 M KCl. The Hamaker constant is 5 kT. Two sets of calculations are shown in Figs. 7 and 8; in one set, the DLVO potentials and the specific-interaction potential are used and in the other, only the hard-sphere and specific-interaction potentials are included. As pH rises, well depth, ε_{spec} increases for both calculations (see Fig. 7). Fig. 8 shows that ε_{spec} increases with sodium-chloride concentration for both models.

6.4. Circular-dichroism (CD) spectropolarimetry

CD spectra were obtained as a function of pH at 25°C with peptide concentrations in the range 5–10 μM. Because the buffer contribution to the molar ellipticity was significant with a 25 mM sodium phosphate buffer, these measurements were taken in a 5 mM buffer. Results are shown in Fig. 9. The CD spectrum at pH 4 has a minimum at 197 nm, consistent with the peptide having a random coil conformation [21]. This spectrum is similar to that obtained by Najbar et al. [22] at pH 4.8 in a 10 mM potassium phosphate buffer. As pH increases to 7, the spectrum develops a minimum at 216 nm, indicating that the peptide adopts a β-strand conformation [21].

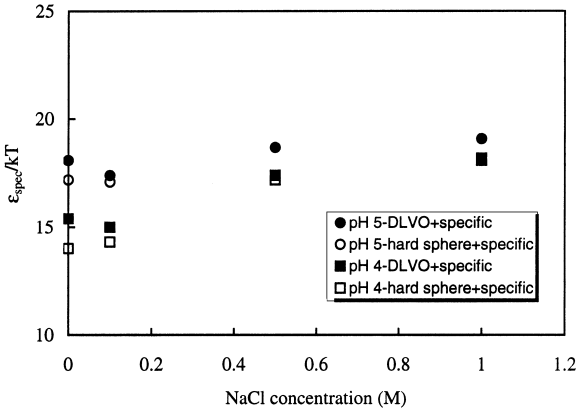

Fig. 8. Square-well depth, ε_{spec}, as a function of NaCl concentration.

7. Discussion

7.1. Strength of interaction

Interactions between the peptide molecules are driven by attractive forces similar to those observed for various proteins known to undergo

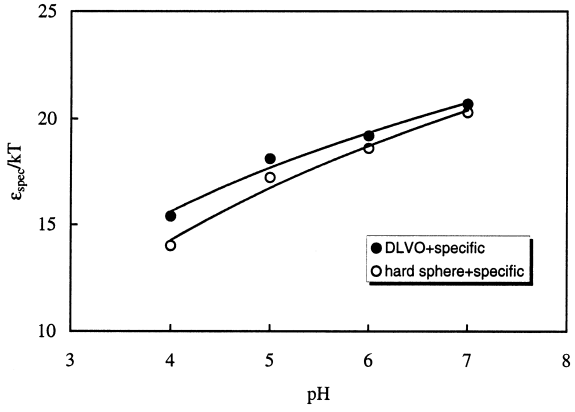

Fig. 7. Square-well depth, ε_{spec}, as a function of pH. NaCl concentration is zero. A spline fit is used to guide the eye.

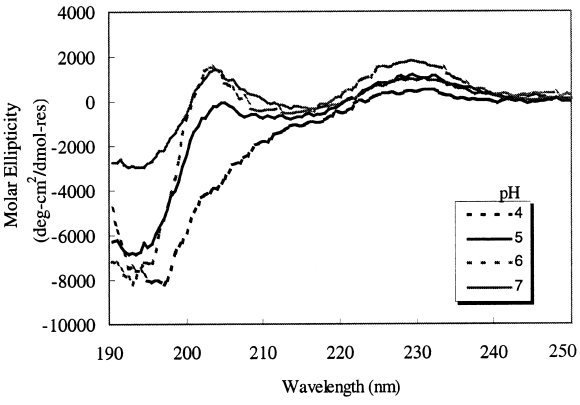

Fig. 9. Far-UV CD spectra of the T4 LYS(11–36) peptide in a 5 mM sodium phosphate buffer at 25°C.

amyloid fibrillogenesis. The observed well depths of the specific interaction potential, ε_{spec}, are in the range 14–20 kT. At 18°C, this corresponds to bond energies on the order of 34–48 kJ/mol. The strength of a hydrogen bond is approximately 13–30 kJ/mol, while a covalent C–C bond has a dissociation energy of 347 kJ/mol [23]. The strength of an intramolecular salt bridge can range from zero if it is on the surface, to 21 kJ/mol if it is buried [24]. For a hydrophobic molecule with a diameter of 18.8 Å, the hydrophobic free energy of dimerization is −38 kJ/mol [18].

It is possible that the attractive interaction is due to the formation of hydrogen bonds or salt bridges. There are a number of amino acids in the peptide that could participate in such interactions (see Appendix A). Alternatively, a hydrophobic bond could be responsible for the strong attraction. There are 10 amino acids in the sequence that can readily participate in hydrophobic interactions.

7.2. pH dependence of interaction

Increased association is observed with rising pH. The well depth is a stronger function of pH than of ionic strength. Fig. 7 shows that there is an appreciable difference in the ε_{spec} values obtained when the electric double layer is included compared to when it is neglected. At pH 4, where the peptide molecules have the highest charge, there is a large discrepancy between the two models. At pH 7, where the molecules have the smallest net charge, there is less difference, indicating that it is necessary to include the electric double-layer-repulsion potential in the model. Inclusion of this potential does not greatly affect the strong pH dependence of the well depth. Thus, there must be some other intermolecular forces that induce the observed pH-dependent interaction. Short-range electrostatic forces may be responsible, in the form of multiple salt bridges. Alternately, hydrogen bonds could cause this strong attraction. It may be that the interaction is not affected by the net charge of the molecule, but rather by the charges on the amino acids that are responsible for binding.

7.3. Role of structure in association

An increase in secondary structure is another consequence of increasing pH. The formation of β-structure may drive the interaction, suggesting hydrogen-bond formation as the cause of attraction between peptide molecules.

7.4. Ionic-strength dependence of interaction

Association also increases with sodium chloride concentration. Fig. 8 shows that at low ionic strength there is a difference in the ε_{spec} values obtained when the electric double layer is taken into account and when it is not. As the ionic strength increases to 1.0 M NaCl, the differences between the two models decline. There is a larger difference between the models at pH 4 than at pH 5. The difference between the models indicates that screening of the overall charge occurs as the ionic strength increases.

If association in this system is due to short-range electrostatic interactions, these should be screened out as the ionic strength increases, causing a decrease in attraction rather than the observed increase. The ionic-strength dependence of association may be due to the effect of salt on hydrophobic interactions. The effect of salt type on the surface tension of water follows the lyotropic series [25]. If the specific interactions in this system are due to interactions between hydrophobic patches, an increase in the surface tension of water would lead to a decrease in protein surface–water contacts, or in effect, stronger peptide–peptide attraction. Na^+ and Cl^- ions are intermediate in the lyotropic series, indicating that neither has a strong tendency to increase the surface tension of water.

8. Conclusions

This work describes interactions of the peptide T4 LYS(11–36) measured by fluorescence anisotropy. The association constants increase with pH and sodium chloride concentration. The observed dimerization equilibrium constants can be described by a potential of mean force consist-

ing of the DLVO potentials and a specific interaction potential. It was shown that specific interactions play a large role in the interactions of the peptide T4 LYS(11–36).

Acknowledgements

This work was supported by the Director, Office of Science, Office of Basic Energy Sciences Chemical Sciences Division of the US Department of Energy under Contract Number DE-AC03-76SF00098. Additional support was provided by the National Science Foundation under Grant Number CTS 9530793. We thank David King for the synthesis, purification and analysis of the unlabeled and labeled peptides.

Appendix A

Experimental procedures

A.1. Peptide synthesis

T4 LYS(11–36), which has the amino acid sequence EGLRLKIYKDTEGYYTIGIGHLLTKS, was assembled on an Applied Biosystems 431A synthesizer using the Fmoc (9-fluorenylmethoxycarbonyl) group for protection of the α-amino function (Dr David King at the Howard Hughes Medical Institute Peptide/Mass Spectrometry Laboratory). The peptide was cleaved from the resin and deprotected with reagent K. The crude product was purified by reversed-phase, high-performance liquid chromatography using an acetonitrile–water–TFA (trifluoroacetic acid) mixture. Approximately 1 mol TFA per positive charge and 20% H_2O were present in the lyophilized peptide powder. Electrospray ionization mass spectrometry yielded a molecular weight of 2969.4 Da, consistent with the theoretical value. The peptide has an isoelectric point of 9.9.

A.2. Conjugation of fluorescent label

7-Methoxycoumarin-3-carboxylic acid (Molecular Probes, Inc., Eugene, Oregon, cat# M-1420) was attached to the N-terminus of the protected peptide on the resin by activation with HBTU/HOBt (hydroxybenzotriazol-1-yl tetra-methyluronium hexafluorophosphate/1-hydroxybenzotriazole). Electrospray ionization mass spectrometry yielded a molecular weight of 3171.7 Da.

A.3. Sample preparation

Water used to prepare the sample solutions was filtered through a Barnstead Nanopure Water Purification System. Sodium chloride (cat# S271-500), sodium phosphate dibasic heptahydrate (cat# S373-500) and sodium phosphate monobasic monohydrate (cat# S369-500) were purchased from Fisher Scientific Company, Pittsburg, PA, USA. Cellulose ester dialysis membranes with a nominal molecular weight cutoff of 1000 Da (cat# 131 087) were purchased from Spectrum®, Laguna Hills, CA, USA. Buffer solutions were prepared by dissolving suitable amounts of monobasic sodium phosphate, dibasic sodium phosphate and sodium chloride in 1 l Nanopure water. The solutions were adjusted to the desired pH with sodium hydroxide or phosphoric acid solutions.

Peptide solutions for fluorescence polarization measurements were prepared such that the mole ratio of fluorescently-labeled to unlabeled peptide was 1:9. This ratio was optimal for ensuring that there was sufficient fluorescent signal for measurement, while at the same time ensuring that the fluorophore concentration was below the level where fluorescence transfer between fluorophores would occur. The solubility of the peptide was greatest at pH 4 in a 25 mM sodium phosphate buffer. Therefore, 1-ml peptide solutions with a concentration of 160 μM were made in 25 mM sodium-phosphate buffer at pH 4 and dialyzed overnight against 1 l of the buffer or salt solution of interest. Dialysis also served to dilute the trifluoroacetic acid (TFA) present in the lyophilized peptide by 1000-fold. This was advantageous, as TFA drastically changes the pH of peptide solutions.

After dialysis, the pH was adjusted to the correct value using either 10–20 μl of 8.5×10^{-5} g/g phosphoric acid or 10–20 μl of 0.5 M sodium

hydroxide. The 160 μM peptide solution was diluted with buffer to obtain solutions in the concentration range 0.5–160 μM. The solutions were allowed to equilibrate for 2 h before the anisotropy was measured.

A.4. Fluorescence-anisotropy measurements

Fluorescence anisotropy was measured on a SLM 4800S Spectrofluorimeter using the L-format [10]. Excitation was measured at 360 nm and emission was measured at 404 nm, based on excitation and emission spectra obtained for the coumarin-labeled peptide (unpublished results).

A.5. Correction of anisotropy values

To eliminate background fluorescence, the intensities of the horizontally and vertically polarized components of the buffer were measured and subtracted from the intensities of the peptide solutions before the anisotropy was calculated.

The viscosity of the buffer solution increased slightly due to increasing salt concentration. To measure aggregation, only the effect of changes in molar volume on the anisotropy are of interest. Therefore, the anisotropy was corrected using the viscosity of pure water, η_o, and the viscosity of the salt solution, η:

$$A_{\text{corrected}} = A_{\text{observed}} \cdot \frac{(1 + RT\tau/\eta V)}{(1 + RT\tau/\eta_o V)} \qquad \text{(A.1)}$$

Values for η and η_o were obtained from the CRC Handbook of Chemistry and Physics [26]. The fluorescence lifetime used in the calculation was $\tau = 3.01$ ns (personal communication, Molecular Probes, Inc.). The molar volume was calculated using a number-average molecular weight, because the peptide solutions contain both labeled and unlabeled peptide. The partial specific volume, $\bar{v}$, was estimated to be 0.7 ml/g, based on values for a variety of proteins [24]. The hydration, $h = 0.2$ g H_2O/g peptide, obtained from Lakowicz [10], was converted to milliliter per gram using the appropriate solution density.

A.6. Circular-dichroism (CD) spectropolarimetry

It was not possible to obtain spectra under the solution conditions used for fluorescence polarization measurements because of the large signal of the sodium chloride and the 25 mM sodium phosphate buffer. Thus, unlabeled peptide solutions were prepared in a 5 mM sodium phosphate buffer. Peptide concentrations were between 5 and 10 μM. CD spectra were recorded at 25°C on an Aviv Model 62DS circular-dichroism spectropolarimeter using a 1-cm pathlength cuvette. The wavelength range was 190–250 nm, with intervals of 0.5 nm and a bandwidth of 1.5 nm. Mean molar ellipticities (degree-cm^2/dmol-residue) are shown in Fig. 9.

A.7. Peptide concentration measurements

Concentrations were measured using a Beckman DU640 Spectrophotometer. The total molar concentration of labeled peptide, $[L^*]_T$, was derived from the absorbance at 360 nm (the wavelength of maximum absorbance of the fluorophore) and the fact that only one fluorophore was conjugated to a peptide molecule:

$$[L^*]_T = \frac{A_{360}}{\varepsilon_c l} \qquad \text{(A.2)}$$

where A_{360} is the absorbance measured at a wavelength of 360 nm and ε_c is the extinction coefficient of the coumarin label; $\varepsilon_c = 16\,000$ M/cm (personal communication, Molecular Probes, Inc.). The pathlength of the cuvette is, $l = 1$ cm. The total peptide concentration was calculated by:

$$[\Lambda]_T = [L]_T + [L^*]_T = \frac{A_{280} - 0.16A_{360}}{\varepsilon_L l} \qquad \text{(A.3)}$$

where A_{280} is the absorbance measured at 280 nm. The extinction coefficient of the peptide, ε_L, was estimated from the absorbance of aromatic groups in a 0.02 M phosphate buffer at pH 6.5 and 6.0 M guanidinium hydrochloride [27]. The

peptide contains three tyrosine groups, thus ε_L = 3840 M/cm. The correction factor, 0.16, was included to compensate for absorption of the coumarin label at 280 nm (personal communication, Molecular Probes, Inc.).

A.8. Calculation of peptide diameter

The effective spherical diameter of the peptide was calculated using the relation [24].

$$\sigma = 2\left(\frac{3M\bar{v}}{4\pi N_A}\right)^{1/3} \quad \text{(A.4)}$$

where the peptide molecular weight, M, is 2969 g/mol, and the partial specific volume of the peptide, $\bar{v}$, is 0.7 ml/g. N_A is Avogadro's number.

A.9. Accuracy of fit

Figs. 2–4 show the best-fit curves to the data using Eq. (13). When there is no sodium present, as in Fig. 2, the fit is excellent. R^2 values are greater than 95%. At increasing salt concentration, the fit becomes less accurate. The R^2 values for curves at pH 4 fall from 83 to 76% as the sodium-chloride concentration increases from 0.1 to 1.0 M (see Fig. 3). At pH 5, R^2 ranges from 75 to 92%. Lowered accuracy of fit may be due to the formation of higher aggregates than dimers at higher ionic strengths. Our model does not account for the existence of such oligomers. To model more accurately the peptide–peptide interactions, these higher aggregates would have to be considered.

References

[1] D.M. Walsh, A. Lomakin, G.B. Benedek, M.M. Condron, D.B. Teplow, Amyloid β-protein fibrillogenesis: detection of a protofibrillar intermediate, J. Biol. Chem. 272 (1997) 22364–22372.

[2] J.D. Harper, C.M. Lieber, P.T. Lansbury, Atomic force microscopic imaging of seeded fibril formation and fibril branching by the Alzheimer's disease amyloid β-protein, Chem. Biol. 4 (1997) 951–959.

[3] C.-L. Shen, R.M. Murphy, Solvent effects on self-assembly of β-amyloid peptide, Biophys. J. 69 (1995) 640–651.

[4] D.R. Booth, M. Sunde, V. Bellotti et al., Instability, unfolding and aggregation of human lysozyme variants underlying amyloid fibrillogenesis, Nature 385 (1997) 787–793.

[5] J.J. Yang, M. Pitkeathly, S.E. Radford, Far-UV circular dichroism reveals a conformational switch in a peptide fragment from the β-sheet of hen lysozyme, Biochemistry 33 (1994) 7345–7353.

[6] A. Einstein, Zur theorie der Brownschen bewegung, Ann. Phys. 19 (1906) 371–381.

[7] K.L. Bentley, L.K. Thompson, R.J. Klebe, P.M. Horowitz, Fluorescence polarization: a general method for measuring ligand binding and membrane microviscosity, BioTechniques 3 (1985) 356–366.

[8] G. Weber, Rotational Brownian motion and polarization of the fluorescence of solutions, Adv. Prot. Chem. 8 (1953) 415–459.

[9] J.R. Lundblad, M. Laurence, R.H. Goodman, Fluorescence polarization analysis of protein–DNA and protein–protein interactions, Mol. Endocrinol. 10 (1996) 607–612.

[10] J.R. Lakowicz, Principles of Fluorescence Spectroscopy, Plenum Press, New York, 1983, p. 5.

[11] M.F. Perrin, Polarisation de la lumiére de fluorescence. Vie moyenne des molécules dans l'état excité, J. Phys. Radium 6/7 (1926) 390–401.

[12] G. Weber, Polarization of the fluorescence of macromolecules: 1 theory and experimental method, Biochem. J. 51 (1952) 145–155.

[13] A.L. Fink, Protein aggregation: folding aggregates, inclusion bodies and amyloid, Folding Des. 3 (1998) R9–R23.

[14] H.A. Havel, E.W. Kauffman, S.M. Plaisted, D.N. Brems, Reversible self-association of bovine growth hormone during equilibrium unfolding, Biochemistry 25 (1986) 6533–6538.

[15] R.A. Curtis, J.M. Prausnitz, H.W. Blanch, Protein–protein and protein–salt interactions in aqueous protein solutions containing concentrated electrolytes, Biotechnol. Bioeng. 57 (1998) 11–21.

[16] E.J.W. Verwey, J.T.K. Overbeek, Theory of Lyophobic Colloids, Elsevier, Amsterdam, 1948.

[17] S. Nir, Van der Waals interactions between surfaces of biological interest, Prog. Surf. Sci. 8 (1976) 1–58.

[18] J. Israelachvili, Intermolecular and Surface Forces, 2nd, Academic Press, San Diego, 1991, pp. 132–199.

[19] M.S. Wertheim, Fluids of dimerizing hard spheres and fluid mixtures of hard spheres and dispheres, J. Chem. Phys. 85 (1986) 2929–2936.

[20] D. Chandler, Introduction to Modern Statistical Mechanics, Oxford University Press, New York, 1987, pp. 211–212.

[21] R.W. Woody, Theory of circular dichroism of proteins, in: G.D. Fasman (Ed.), Circular Dichroism and the Conformational Analysis of Biomolecules, Plenum Press, New York, 1996.

[22] L.V. Najbar, D.J. Craik, J.D. Wade, D. Salvatore, M.J. McLeish, Conformational analysis of LYS(11–36), a

peptide derived from the β-sheet region of T4 lysozyme, in TFE and SDS, Biochemistry 36 (1997) 11525–11533.
[23] L. Stryer, Biochemistry, 3rd, W.H. Freeman and Company, New York, 1988.
[24] T.E. Creighton, Proteins: Structures and Molecular Properties, 2nd, W.H. Freeman and Company, New York, 1993.
[25] W. Melander, C. Horváth, Salt effects on hydrophobic interactions in precipitation and chromatography of proteins: an interpretation of the lyotropic series, Arch. Biochem. Biophys. 183 (1977) 200–215.
[26] R.C.Weast (Ed.), CRC Handbook of Chemistry and Physics, 67th ed., CRC Press Inc, Boca Raton, Florida, 1986 pp. D253–D254.
[27] Swiss-Protein Database. http://expasy.hcuge.ch/cgi-bin/protparam.